Adapted parameterization of incomplete ionization in aluminum-doped silicon and impact on numerical device simulation

Heiko Steinkemper,[1,a)] Michael Rauer,[1] Pietro Altermatt,[2] Friedemann D. Heinz,[1] Christian Schmiga,[1] and Martin Hermle[1]
[1]*Fraunhofer Institute for Solar Energy Systems ISE, Heidenhofstrasse 2, 79110 Freiburg, Germany*
[2]*Department Solar Energy, Institute Solid-State Physics, University of Hannover, Appelstrasse 2, 30167 Hannover, Germany*

(Received 30 September 2014; accepted 8 February 2015; published online 20 February 2015)

The amount of incomplete ionization of aluminum-doped silicon is measured at room temperature by comparing electrochemical capacitance-voltage measurements with micro Raman spectroscopy. It is shown that commonly used parameterizations significantly underestimate the effect of incomplete ionization in Al doped Si. Based on the experimental data, we propose new parameter values for the parameterization of incomplete ionization given in Altermatt *et al.*, J. Appl. Phys. **100**, 113715 (2006). Using these new values, the saturation current density $J_{0,p+}$ of the Al-alloyed region of a standard silicon solar cell is determined by means of numerical device modeling. It is shown that the parameterization influences $J_{0,p+}$ significantly. Additionally, the weakening effect of incomplete ionization on band gap narrowing (BGN) should be taken into account in modeling that aims to predict device behavior after changes made to the Al-alloyed region. © *2015 AIP Publishing LLC*. [http://dx.doi.org/10.1063/1.4913255]

I. INTRODUCTION

Today's standard (or more advanced) industrial crystalline silicon solar cells feature full-area (or local area) aluminum-doped p^+ (Al-p^+) silicon regions on the back (often referred to as back-surface-field or BSF) and full-area (or local) rear contacts. Even though it is industrial standard and therefore well-investigated, numerical device simulation of Al-p$^+$ regions is still a challenging task. In the past, the calculated saturation current density of Al-p^+ regions, $J_{0,p+}$, have been far too low compared to the experimentally determined values.[1] Therefore, a parameterization was introduced for the Shockley-Read-Hall lifetime, which is reduced due to the formation of aluminum-oxygen complexes in the Al-p^+ region,[2,3] in order to achieve more realistic $J_{0,p+}$ values.[1] However, it was pointed out by Rüdiger *et al.* that this approach is not sufficient for highly Al-doped silicon and the effect of incomplete ionization has to be considered to accurately describe the $J_{0,p+}$ of Al-p^+ regions.[4]

Incomplete ionization in Al-p^+ regions becomes relevant at dopant densities (N_{dop}) above about 5×10^{16} cm^{-3}, where the Fermi level E_F starts to approach the dopant level sufficiently close so that a significant portion of the dopant states becomes occupied, and therefore the free carrier density becomes significantly lower than N_{dop}. The effect of incomplete ionization directly depends on the ionization energy of the dopant species E_{dop}. At high doping concentrations, E_{dop} approaches the band edge, resulting in lower ionization energies and, hence, in a smaller portion of occupied dopant states. At a critical dopant density N_{crit} around 10^{19} cm^{-3}, a change of the conductivity behavior can be observed,[5] the so-called metal-insulator (MI) or Mott transition.[6] N_{crit} of the MI transition specifies the dopant concentration for which the dopant band touches the semiconductor band.[7] Above N_{crit}, there exists practically no incomplete ionization (apart from a small density of immobile tail states).

For a quantification of incomplete ionization, E_{dop} needs to be quantified in dependence of N_{dop}. There are various models describing E_{dop} as a function of N_{dop}. A pioneering and frequently used model was presented by Pearson and Bardeen in 1949.[8] In 2006, it was shown that the model of Pearson and Bardeen significantly deviates from an extensive collection of experimental data for boron-, phosphorus-, and arsenic-doped silicon.[7,9] Therefore, an advanced parameterization for E_{dop} was introduced based on theories and experiments from the literature.[7,9] In Al-doped regions, at low doping concentrations, $E_{dop,0}$ is significantly higher (69.03 meV)[10] than $E_{dop,0}$ of boron acceptors (44.39 meV)[10] and phosphorus donors (45.5 meV),[11,12] Therefore, it is expected that the ionization fraction of Al for N_{dop} close to the MI transition is significantly lower than for B and P.[4,13] Hence, a correct parameterization of E_{dop} and the caused incomplete ionization fraction are even more important for Al-doped Si. However, in contrast to B- or P-doped Si, there has been only very sparse experimental data available for Al-doped silicon, which has impeded the determination of accurate parameterizations. In this paper, we determine the fraction of ionized Al acceptors in Al-doped Si directly by comparing the doping profiles measured using the electrochemical capacitance-voltage (ECV) technique[14,15] and using micro Raman spectroscopy[16] (μRS). Based on these experiments, we choose parameters for the parameterization given in Ref. 9 and, finally, determine the influence of incomplete ionization on $J_{0,p+}$ by means of numerical device modeling.

[a)]Author to whom correspondence should be addressed. Electronic mail: heiko.steinkemper@ise.fraunhofer.de. Phone: +49 0761 4588-5097.

II. INCOMPLETE IONIZATION

A. Theory

In this work, we focus on Al acceptors in silicon and therefore discuss the theory only for acceptors. Nevertheless, the presented formalism is similarly valid for donors as well.

The total acceptor concentration N_A is the sum of the ionized acceptor concentration N_A^- and of the non-ionized acceptor concentration, N_A^0. The fraction of the ionized acceptor concentration, f_A, is given by[17]

$$f_A(N_A) = \frac{N_A^-}{N_A} = \frac{1}{1 + g_A \exp\left(\frac{E_A(N_A) - E_{Fp}(N_A)}{kT}\right)}, \quad (1)$$

which differs from the Fermi-Dirac distribution by the degeneracy factor g_A.[18] Since both the ionization energy E_A as well as the quasi Fermi level E_{Fp} depend on N_A, Eq. (1) has to be solved iteratively. The importance of the ionization energy E_A was already pointed out in the introduction. Therefore, we take a closer look at the models which are commonly used to describe $E_A(N_A)$. E_A decreases with increasing N_A, which was explained by Pearson and Bardeen[8] with the potential energy due to the Coulomb attraction between ionized acceptors and holes in the valence band. Thus, the decrease of E_A is taken as inversely proportional to the average distance between the impurities and is therefore expressed by[8]

$$E_A^{P\&B} = E_{A,0} - \alpha N_A^{(1/3)}. \quad (2)$$

Debye and Conwell[19] pointed out that there are additional reasons for a decrease of E_A: screening of the electric field around charged centers by free carriers[20] and polarization effects.[21]

Therefore, the logistical equation was taken to parameterize $E_A(N_A)$[7,9]

$$E_A^{Alt}(N_A) = \frac{E_{A,0}}{1 + \left(N_A/N_{ref}\right)^c}, \quad (3)$$

with the constants N_{ref} and c being characteristic for the kind of dopant. E_A^{Alt} is close to $E_{A,0}$ for low doping concentrations $N_A \ll N_{ref}$, it equals half the ground state doping energy ($E_{A,0}/2$) for $N_A = N_{ref}$, and approaches 0 for $N_A \gg N_{ref}$. The parameter c affects the gradient of E_A^{Alt} under variation of N_A. It has been shown in the literature that Eq. (3) matches the experimental data for phosphorus doping[6] far better than Eq. (2) of Pearson and Bardeen and shows good agreement for boron doping as well.[7,9]

As the general formalism[7] of incomplete ionization is not suitable for numerical device simulation, a simplified model was suggested in Ref. 9

$$f_A^{Alt} = \frac{N_A^-}{N_A} = 1 - \frac{bp}{p + g_A N_V \exp\left(\frac{-E_A^{Alt}(N_A)}{kT}\right)}, \quad (4)$$

using

$$b = \frac{1}{1 + (N_A/N_b)^d}, \quad (5)$$

with the constants N_b and d dependent on the dopant species and the effective density of states in the valence band at 300 K, $N_V = 3.1 \times 10^{19}\,\mathrm{cm}^{-3}$, as determined by Green.[22] Equation (5) has the same form as Eq. (3). Therefore, the parameter b is close to 1 for low doping concentrations $N_A \ll N_b$, it equals 1/2 for $N_A = N_b$ and approaches 0 for $N_A \gg N_b$. The parameter d affects the slope of the change from 1 to 0. In this work, solely the simplified model will be used, since on the one hand the aim is to find a parameterization for numerical device simulation, and on the other hand the deviations from the general model are negligible compared to the scatter of the experimental data.[9]

At this point, it should be emphasized that one has to be careful with the definition and the values of the degeneracy factor g_A. Reference 9 on the one hand reported degeneracy factors of $g_A = 1/4$ for acceptors (Eq. (4)) and $g_D = 1/2$ for donors[7,9] and on the other hand degeneracy factors of 4 (Eq. (1)) and 2, respectively, can be found in the literature.[17,23] This is due to different definitions of Eqs. (1) and (4) by means of an inverse degeneracy factor g^{-1}. While the degeneracy factors are always the same result of the electron spin, and in the case of acceptors, degeneration of the valence and impurity band, the used definitions and values of the degeneracy factors are not always consistent.[7,17,23–25]

B. Experimental determination of the ionization fraction of aluminum dopants in silicon

The investigation of incomplete ionization of boron-, phosphorus-, and arsenic-doped silicon in Refs. 7 and 9 was based on an extensive collection of experimental data found in the literature. In contrast to this abundance of data for these dopant types, there is only sparse data available for Al-doped Si.[26–30] Therefore, we introduce here a straight forward approach to directly access the ionization fraction of Al-doped Si.

We prepared Al-p^+ regions by alloying of screen-printed Al paste on Si wafers in a short firing step at a set peak temperature of 900 °C, as typically applied in the fabrication of Si solar cells.[31] The Al-p^+ regions are thereby formed by the incorporation of Al atoms into the recrystallizing Si according to the solid solubility of Al in Si.[32] Thus, the Al concentration of alloyed p^+ regions is typically in the range of 7×10^{17} to $5 \times 10^{18}\,\mathrm{cm}^{-3}$. This doping concentration range is highly relevant for incomplete ionization.

We have fabricated simple test samples using shiny-etched (100)-oriented B-doped p-type Si wafers. The wafers were wet-chemically cleaned and an Al paste was screen-printed onto one entire wafer surface.[13,31] The Al-p^+ regions were subsequently formed during alloying in a conveyor belt furnace at a set peak temperature of 900 °C. Different peak temperature times have been applied causing a different Al-p^+ region thickness for each of the samples.[33,34] The corresponding, measured sheet resistances of the investigated samples are 23 Ω/sq, 36 Ω/sq, and 57 Ω/sq. Finally, the paste residuals and Al-Si eutectic layers were removed by etching in hydrochloric acid. To determine the percentage of ionized Al acceptors in Si, we applied the following two methods:

(i) Electrochemical capacitance-voltage (ECV) measurements: ECV measurements detect the *total* Al dopant concentration (ionized and non-ionized Al acceptors) in Si.[13,31,35] The ECV technique is based on creating a Schottky contact between the Al-doped Si surface and an electrolyte, which leads to the formation of a space charge region (SCR) within the Si. By differentially modulating an external voltage on this Schottky contact and measuring the capacitance of the SCR, the acceptor concentration at the edge of the SCR can be determined.[15] Since the strong band bending within the SCR leads to the ionization of non-ionized Al acceptors,[13,31,35] ECV detects the *total* concentration of Al acceptors. This was recently confirmed by comparing profiles of Al-p^+ regions measured by secondary ion mass spectrometry (SIMS) and ECV, which are in good agreement.[31]

(ii) micro-Raman spectroscopy (μRS): The doping density of the *ionized* Al acceptors can be measured by detecting Raman scattered light. The Raman Stokes peak at 521 rel. cm^{-1} is asymmetrically broadened due to Fano resonance of scattering at phonons and at the electron or hole plasma.[36] The plasma density depends on the doping density, and thus a dependence of half width and asymmetry of the Raman Stokes peak on doping density can be found.[37] Due to the sensitivity of the method to the free carrier density, only the ionized Al acceptors are detected.

We used epitaxially grown boron-doped Si layers with known doping concentrations to calibrate the half width of the Raman Stokes peak to ionized doping densities. The implementation of this Fano resonance-based method into a confocal microscope setup is called micro-Raman spectroscopy (μRS) and allows for the measurement of ionized acceptor densities with diffraction limited spatial resolution of down to 200 nm for doping densities above $9 \times 10^{16}\,cm^{-3}$.[16] The spatial resolution of μRS which is based on a spot wise measurement due to the confocal setup is established by raster scanning the cross section of the sample with a piezo stage. The calibration of the absolute depth of the doping profile, i.e., the determination of its relative distance to the physical sample edge, is extracted directly from the Raman scattering intensity which linearly correlates to the scattering volume. The laser spot profile has a Gaussian shape, thus the intensity of the scattered light drops at the edge of the sample according to an error function. A fit to the intensity profile at the sample edge yields a precise determination of the sample surface position with an error less than 100 nm.

μRS was applied to Al-p^+ regions to measure the profiles of *ionized* Al acceptors. Cross-sections of the samples were prepared and mechanically chemically polished for this purpose. Several linescans along the normal to the Al-p^+ region surface were recorded to detect the profiles.

The results of one ECV measurement and three μRS Al doping profile measurements carried out on the same sample only few millimeters apart are plotted in Fig. 1 (left, open black and filled green squares, respectively). The ECV-measured Al doping profile shows a characteristic decrease from the Si base/Al-p^+ region interface toward the surface, because the alloy recrystallizes towards the surface with decreasing temperature and, hence, decreasing Al solubility.[38]

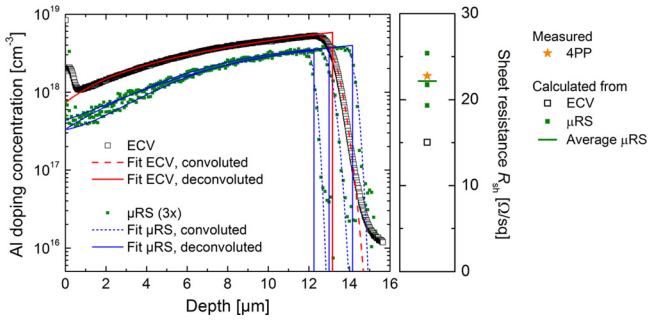

FIG. 1. Left: Al doping profiles measured on the same sample by ECV (open black squares) and μRS (green squares). The μRS measurements were carried out at three different positions. The profiles feature no abrupt decrease at the Al-p^+/Si-transition due to Al-p^+ thickness inhomogeneities within the measurement area. The profiles are fitted (dashed lines) by assuming a convolution of the actual profile (solid lines) with a Gaussian thickness distribution to account for the inhomogeneities. Right: The sheet resistance R_{sh} of the sample determined by 4PP measurement (orange star) compared with the calculated R_{sh} based on the ECV profile (open black square), the μRS profiles (green squares) and the average R_{sh} of the μRS profiles (green line). Very good agreement of the calculated average and the 4PP measurement is shown.

Two additional features appear, which are typical for ECV measurements of alloyed Al-p^+ regions: (1) an artifact peak near the surface of the p^+ region, which can be attributed to small pyramidal structures on the surface,[39] and (2) a blurring of the Si base/Al-p^+ region transition, which is caused by the superposition of various Al-p^+ region thicknesses within the ECV measurement spot exhibiting a diameter of 3.55 mm.[13,31] These thickness variations are expected to originate from a laterally inhomogeneous distribution of Si in the Al-Si melt which occurs since the dissolution of Si from the wafer surface starts locally at the positions where the Al paste particles are in direct contact with it.[40] The Al-Si melt thus exhibits lateral fluctuations leading to a Gaussian-distributed thickness variation of the Al-doped p^+ Si region during recrystallization.[13] The ECV-measured Al dopant profile can therefore be fitted by neglecting the artifact peak near the surface and convoluting an abrupt dopant profile with a Gaussian thickness distribution.[13,31] Fig. 1 (left) shows that the fitted curve accurately describes the ECV-measured profile. The abrupt, deconvoluted profile then represents the actual Al dopant profile for the mean Al-p^+ region thickness.[13,31]

As stated before, μRS linescan measurements were performed at three different spots of the same sample to account for the higher resolution compared to the ECV technique. Due to the smaller μRS measurement spot diameter of only 500 nm, the Al dopant profiles show a much steeper decrease of the Al-p^+/Si base transition and each profile exhibits a different thickness within the Gaussian distribution of the ECV measurement. Similar results have been shown recently for SIMS-measured profiles.[31]

For the comparison of the μRS-measured concentration of ionized Al acceptors and the ECV-measured total Al concentration, we use the corresponding calculated, deconvoluted profiles (solid lines) each featuring a certain depth. This approach accounts for the Al-p^+ thickness variations as discussed before. The fraction of the ionized concentration relating to the total concentration gives us the incomplete

ionization fraction as defined in Eqs. (1) and (4), respectively. Our experimentally determined ionization fraction of these multiple measurements at three different samples is plotted in Fig. 2 as symbols.

Fig. 1 (right) shows a comparison of the sheet resistances R_{sh} of the investigated sample determined by four point probe (4PP) measurement (orange star), calculated based on the ECV profile (open black square),[31] the μRS profiles (green squares), and the average R_{sh} of the μRS profiles (green line). The R_{sh} is inverse proportional to the free carrier density and therefore to the ionized Al acceptors. As a consequence, the R_{sh} calculated from the ECV profile taking into account the total acceptor concentration significantly underestimates R_{sh}. Whereas the average R_{sh} of the μRS profiles and the R_{sh} determined by the 4PP measurement are in very good agreement. This confirms the legitimacy of our approach to determine the ionized acceptor concentration by using μRS measurements.

C. New parameterization of the ionization fraction of Al-doped silicon

In Fig. 2, the experimentally determined ionization fraction is compared to the commonly used theoretical parameterization based on Eq. (1) and the ground state doping energy of Pearson and Bardeen (P&B), Eq. (2). Using this parameterization (black dotted line), a critical acceptor concentration N_{crit} for the Mott transition has to be considered with $f_A = 1$ for $N_A > N_{crit}$ (black dashed line in Fig. 2). Otherwise this parameterization would allow for incomplete ionization far beyond the Mott transition which would be physically unreasonable. This leads to a sharp cut-off of the ionization fraction at N_{crit}. $N_{crit} = 8 \times 10^{18}\,cm^{-3}$ for Al-doped silicon was proposed (but not directly measured) by Rüdiger *et al.*[4] and Rauer *et al.*[31] used $N_{crit} = 1.1 \times 10^{19}\,cm^{-3}$. Literature values of other dopant species in silicon,[9] which are plotted in Fig. 3, show a distinct dependence of N_{crit} on

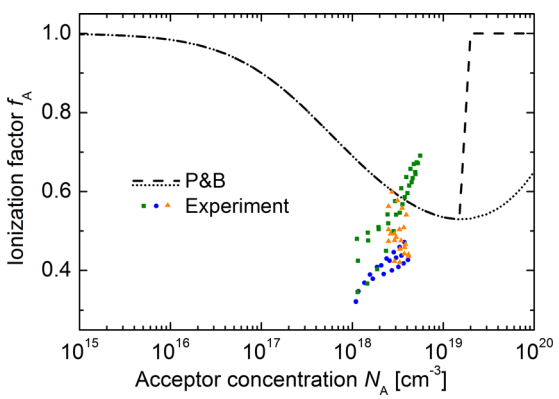

FIG. 2. Experimentally determined ionization fraction f_A of Al dopants in silicon (colored symbols) plotted against the acceptor concentration N_A. For the sake of clarity some measurement points are left out. The different colors correspond to measurements at three different samples. Each of the samples was measured more than once (e.g., the green squares correspond to the three profiles shown in Fig. 1). The experimental data deviate significantly from the parameterization based on the ground state doping energy of Pearson and Bardeen (P&B) which is plotted with and without consideration of a critical density for the Mott transition (black dashed and dotted line, respectively).

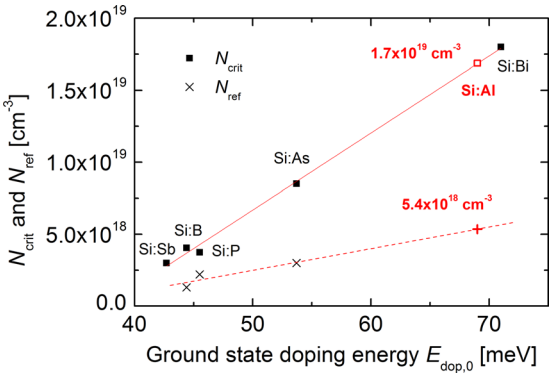

FIG. 3. Filled squares: critical densities N_{crit} for the Mott transition of different dopants in silicon, collected in Ref. 9, plotted against the corresponding ground state energy $E_{dop,0}$, and black crosses: parameter values of N_{ref} from Ref. 9 (values from Table III for device simulation). Linear fits are applied (and in the case of N_{ref} extrapolated to $E_{A1,0}$) to estimate $N_{crit} = 1.7 \times 10^{19}\,cm^{-3}$ for the Mott transition and $N_{ref} = 5.4 \times 10^{18}\,cm^{-3}$ for Al dopants in silicon (empty square and horizontal cross). Since there are only three reference values for N_{ref} over a small energy range, only a rough estimation of N_{ref} is possible.

$E_{dop.0}$. By using a linear regression to this data and $E_{A1,0} = 69.0\,meV$,[10] we estimate an even higher N_{crit} value of $1.7 \times 10^{19}\,cm^{-3}$ for the Mott transition of Al dopants in silicon.

We recommend to abandon the parameterization of Pearson and Bardeen for Al-doped Si, for the following reasons. Good accordance of the experimental data and the parameterization based on the ground state doping energy of Pearson and Bardeen in Fig. 2 can only be observed for N_A values around $3 \times 10^{18}\,cm^{-3}$. The work of Rüdiger *et al.* was based on samples with concentrations of about this order of magnitude, which led to a good accordance of simulation and experiment.[4] The data presented in Fig. 2, however, clearly indicate severe deviations for concentrations lower and higher than $3 \times 10^{18}\,cm^{-3}$. It is evident that a new parameterization for the ionization fraction of Al-doped silicon is needed featuring two important aspects. First, the minimum of the ionized fraction of Al dopants in silicon should be even lower than previously expected from parameterizations based on the ionization energy of Pearson and Bardeen. And second, the minimum of the ionized fraction is located at lower Al concentrations than commonly assumed.

In the following, we fit our experimental data with the parameterization of Ref. 9. There are four free parameters in Eqs. (3) to (5): N_{ref}, c, N_b and d. Note that in Refs. 7 and 9, additional experimental data were available for the ionization energy $E_{dop}(N_{dop})$ of boron and phosphorus in silicon. Therefore, the parameters N_{ref} and c of Eq. (3) could be determined separately. To our knowledge, there is no such data for Al dopants reported in the literature. In order to reduce the number of free parameters of our parameterization and thus minimize the uncertainty of our model, we plot N_{ref} over $E_{dop,0}$ of other dopants in Fig. 3 and proceed in the same way as with N_{crit} (the N_{ref} values are taken from Table III of Ref. 9).

According to the procedure for N_{crit} above, we perform a linear regression to the literature values of N_{ref} and extrapolate to the ground state doping energy of Al. The resulting

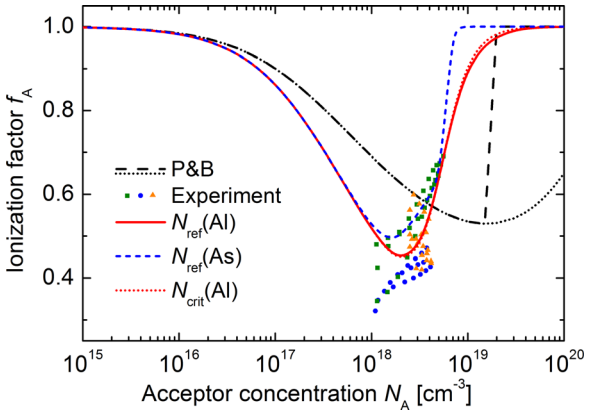

FIG. 4. Ionization fraction f_A of Al dopants in silicon plotted against the acceptor concentration N_A. For the sake of clarity some measurement points are left out. The experimental data are fitted using Eqs. (3) to (5). Three fits featuring different N_{ref} values are plotted: the previously determined $N_{ref}(Al) = 5.4 \times 10^{18}\,cm^{-3}$ (solid red curve), the value of arsenic doped Si $N_{ref}(As) = 3.0 \times 10^{18}\,cm^{-3}$ as a lower limit (dashed blue line), and $N_{crit}(Al) = 1.7 \times 10^{19}\,cm^{-3}$ as an upper limit.

value is $N_{ref} = 5.4 \times 10^{18}\,cm^{-3}$. This is again a rough estimate since there are only three literature values with significantly lower $E_{dop,0}$ than of Al. Since N_{crit} is the concentration were the dopant band touches the valence band[7] and therefore $E_{dop,A}$ approaches zero, it is obvious that $N_{ref} < N_{crit}$.

To determine the remaining free parameters c, N_b, and d we perform a least square fit of our experimentally determined ionization fractions. As starting values we use the values of boron-doped Si determined in Ref. 9. With a fixed $N_{ref} = 5.4 \times 10^{18}\,cm^{-3}$ and no further restrictions to the remaining fit parameters, the parameter c reaches very high values ($c > 10$). This seems very unlikely regarding the much smaller values for boron (1.4), phosphorus (2.0), and arsenic (1.5) doping.[9] Therefore we assume $c \leq 3$ as an upper limit for the following fits plotted in Fig. 4. The fit with $N_{ref}(Al) = 5.4 \times 10^{18}\,cm^{-3}$ and $c \leq 3$ (solid red line) is in sufficiently good agreement with the experimental data. The corresponding fit parameters are listed in Table I.

As stated before, the value $N_{ref}(Al) = 5.4 \times 10^{18}\,cm^{-3}$ is only a rough estimate. Therefore, we perform two further fits to evaluate the influence of N_{ref} on the fit quality:

(i) Lower limit

Arsenic is the dopant with the next lower ground state doping energy ($E_{dop,0} = 53.7$ meV) and an already determined N_{ref} value ($N_{ref}(As) = 3.0 \times 10^{18}\,cm^{-3}$). If we fit our experimental data using a fixed $N_{ref}(As)$, the blue dashed line in Fig. 5 is obtained. It features a sharp bend and, as a result, an unlikely high fit parameter $d > 10$. Further restrictions to the parameter d lead to a negative and therefore unreasonable fit parameter N_b. Hence, the smooth curve of the original fit (solid red curve) arising from the estimated $N_{ref}(Al) = 5.4 \times 10^{18}\,cm^{-3}$ value seems more likely.

TABLE I. Recommended parameter set for the description of incomplete ionization of Al-doped silicon for numerical device simulations using Eqs. (3) to (5).

	Si:Al
$E_{dop,0}$ (meV)	69.0
N_{ref} (cm^{-3})	5.4×10^{18}
c	3.0
N_b (cm^{-3})	5.5×10^{18}
d	2.6
g	1/4

(ii) Upper limit

Using the maximal allowed value $N_{crit}(Al)$ for N_{ref}, the experimental data can still be fitted rather precisely and with reasonable fit parameters as well (dotted red line). This shows that the quality of the fit is rather insensitive to N_{ref} as long as N_{ref} is as high as $N_{ref}(Al)$ Therefore, it seems legitimate to use the fit based on the estimated $N_{ref}(Al) = 5.4 \times 10^{18}\,cm^{-3}$ in Fig. 4.

Finally, the lowest experimentally determined ionization fractions are close to 0.3 at N_A near $1 \times 10^{18}\,cm^{-3}$ whereas our best fit (solid red line) features a minimal ionization fraction of close to 0.4 at N_A of about $2 \times 10^{18}\,cm^{-3}$. In the following, we analyze how the minimal ionization fraction $f_{A,min}$ (and the concentration where it occurs $N_{A,min}$) may be lowered in our parameterization.

The only possibility to achieve a lower $f_{A,min}$ and a lower $N_{A,min}$ simultaneously, is to choose a higher ground state energy $E_{dop,0}$. This is illustrated in Fig. 5 for $E_{dop,0} + \Delta = 80$ meV (dashed black line). However, the ground state energy of Al ($E_{Al,0} = 69.03$ meV) was determined by Fischer and Rome[10] with an uncertainty of only ± 0.02 meV. The adjustment of $E_{dop,0}$ is therefore not a physically reasonable approach to achieve a better agreement between the experimental data and the parameterization.

There are two further possibilities to achieve a lower $f_{A,min}$. The first possibility is adjusting N_{ref} and N_b, see the black dotted line in Fig. 6. With this, $f_{A,min}$ can indeed be lowered, but the parameterization does not describe the overall experimental data any more (due to the increased $N_{A,min}$). A second possibility is to adjust the parameters c and d, as shown by the black dashed-dotted line. However, they mainly affect the slope at $N_A > N_{A,min}$ and not so much $f_{A,min}$.

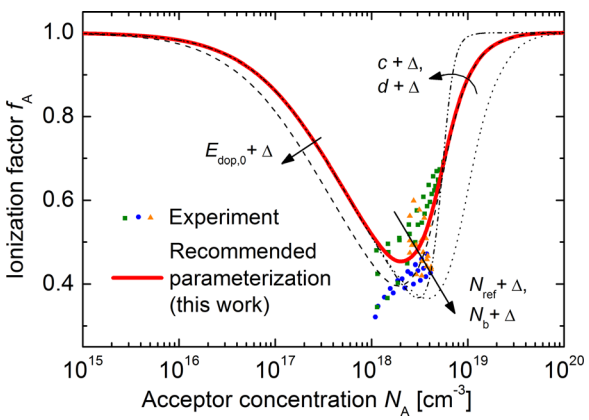

FIG. 5. Analysis of the influence of the free and predefined parameters of the parameterization of incomplete ionization.

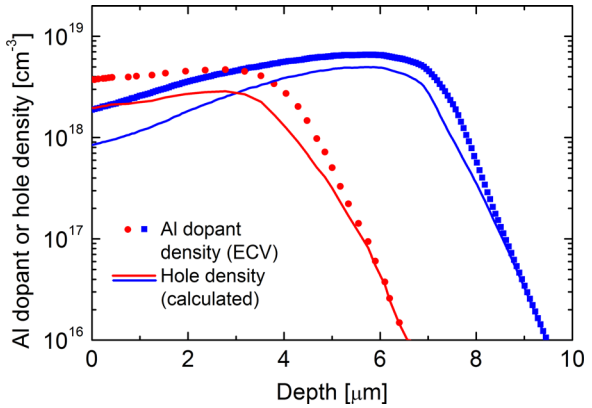

FIG. 6. A 5 μm deep and a 10 μm deep Al dopant profile, measured by ECV (symbols), and the corresponding hole densities (lines), calculated with Eqs. (6) and (7) with the parameters in Table I.

In conclusion, we recommend the parameters listed in Table I (corresponding to the solid red line in Figs. 4 and 5) to describe incomplete ionization of Al acceptors in Si sufficiently accurately for numerical device simulations.

III. IMPACT ON THE SATURATION CURRENT

In the following, we quantify the impact of incomplete ionization on the saturation current density $J_{0,p+}$ of typical Al-alloyed p^+ regions for photovoltaic application by means of numerical device simulations. We use the simulator SENTAURUS DEVICE[23] (SD) and the physical models for crystalline silicon from Ref. 41, with an update[42] by a more recent model for Auger recombination. Incomplete ionization cannot be implemented into SD using Eq. (4) due to software restrictions, but with Eq. (8b) from Ref. 9

$$f_A^{SD} = \frac{N_A^-}{N_A} = \frac{1}{1 + \dfrac{g_A p}{N_V \exp\left(\dfrac{-E_A^{Alt}(N_A)}{kT}\right)}}. \tag{6}$$

E_A is given by Eq. (3) and is a function of N_A. The degeneracy factor g_A, however, loses its physical meaning and becomes a mere compensating factor, given by Eq. (10b) in Ref. 9:

$$g_A(T, N_A) = \frac{b}{g + (1-b)\dfrac{N_A}{N_V \exp\left(\dfrac{-E_A^{Alt}(N_A)}{kT}\right)}}, \tag{7}$$

where b is given by Eq. (5) and is a function of N_A. The resulting incomplete ionization fraction deviates only insignificantly from Eq. (4), compared to the experimental uncertainty.

We extract $J_{0,p+}$ from a simulation of a standard c-Si cell in the following way. The J_0 of the entire solar cell is defined by the Shockley equation of the current-voltage curve in the dark

$$J = J_0\left(\exp\left(\frac{V}{V_{th}}\right) - 1\right), \tag{8}$$

where V_{th} is the thermal voltage, $kT/q \approx 25.8\,\text{mV}$ at 300 K. The J_0 of a local device region can be defined identically, but the external voltage V needs to be replaced by the local voltage V_{loc} at a location x_{loc} in the quasi-neutral region directly in front of the local region

$$J_{loc} = J_{0,loc}\left(\exp\left(\frac{V_{loc}}{V_{th}}\right) - 1\right). \tag{9}$$

Here, the local current J_{loc} is supplied for maintaining the recombination in the local region (provided that the generation of charge carriers in the local region is negligible). Because V_{loc} is identical to the separation of the quasi-Fermi energies $E_{Fn} - E_{Fp}$ at x_{loc}, we can insert the law-of-mass-action,

$$pn = n_{i,eff}^2 \exp\left(\frac{E_{Fn} - E_{Fp}}{V_{th}}\right), \tag{10}$$

into Eq. (9)

$$J_{0,loc} = \frac{J_{loc}}{np - n_{i,eff}^2} n_{i,eff}^2, \tag{11}$$

where all values are taken at x_{loc}. In order to extract $J_{0,p+}$ at V_{loc} relevant to 1-sun condition, we probe these values in our device simulations at the maximum power point (which shifts from near $V = 0.6\,\text{V}$ to 0.53 V depending on $J_{0,p+}$). However, because of our extraction method, the details of the solar cell, such as wafer thickness, wafer resistivity, emitter dopant profile, etc., have only a minor influence on the extracted value of $J_{0,p+}$, as is discussed, e.g., in Ref. 43. To assure that there is no photo-generation occurring within the Al-p^+ region, we truncate the optical generation profile in the Al-p^+ region (the profile is obtained with the am1.5 g spectrum and the ray tracer SUNRAYS[44]).

Fig. 6 shows two typical Al-alloyed p^+ profiles for photovoltaic application found in standard c-Si solar cells: one is 10 μm deep (as typically processed in the laboratory) and the other is 5 μm deep (as typically found in mass production, where the Al-paste consumption is minimized). As described in Sec. II B, the profiles are fabricated by alloying Al and Si during a very short firing step. It is so short that only a fraction f of aluminum-oxygen (Al-O) defects is created compared to the Czochralski crystallization process, used for fabricating Al-doped Si ingots.[2] Still, the Al-O defects influence $J_{0,p+}$ of these profiles strongly.[1,45] Their defect level is therefore included in the simulations with the Shockley-Read-Hall formalism, using the parameters determined in Ref. 46. Fig. 7 shows the simulated $J_{0,p+}$ values in dependence of f, assuming complete ionization of Al dopants (dashed line), and assuming incomplete ionization (dotted line) as given in Eqs. (6) and (7). Incomplete ionization increases $J_{0,p+}$ by over 40% in the whole range of f and, hence, needs to be included in device modelling. This increase is caused by a higher minority carrier density.

However, incomplete ionization also reduces the amount of band gap narrowing (BGN). Generally, BGN depends on N_A^-, N_D^+, p, n, and T, mainly due to Coulomb interaction

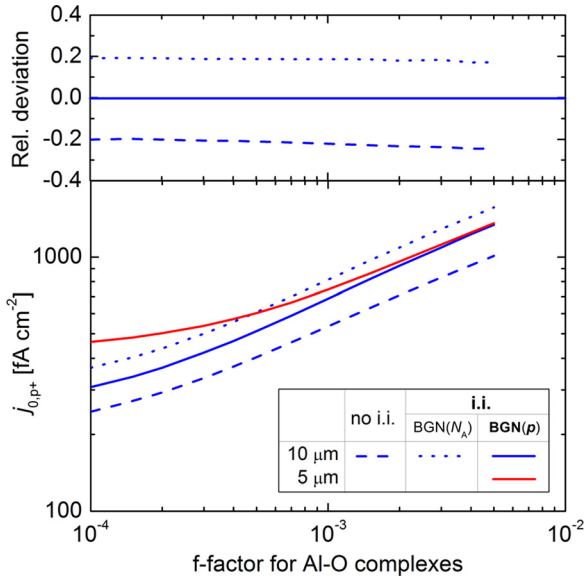

FIG. 7. $J_{0,p+}$ in dependence of the amount (fraction f) of Al-O complexes, simulated with complete ionization (no i.i., dashed line), incomplete ionization (i.i./BGN(N_A), dotted line) using Eqs. (6) and (7), and additionally including the reduction of band gap narrowing (i.i./BGN(p), solid lines), induced by the lower densities of ionized acceptors and holes. In the upper graph, the relative deviation of the hitherto existing models from the improved model featuring the advanced parameterization of this work and the correct consideration of band gap narrowing is shown.

and exchange interaction among the carriers and dopant ions. Incomplete ionization reduces the amount of BGN very effectively, because it removes both ionized dopant ions and majority carriers. We included Schenk's BGN model in SD, concretely using Eqs. (33) and (37) of Ref. 47, and we replaced in its input N_A by p (with the so-called tableBGN feature of SD). The results are given by the solid lines in Fig. 7 and show that $J_{0,p+}$ increases by less but still by about 20% compared to complete ionization. This is still so significant that it should be included in device modelling, if it aims to predict device behavior with changes made to the Al-p$^+$ region.

In the literature, measured $J_{0,p+}$ values are in the range of 250–600 fA/cm^2 (see Ref. 48, p. 137, for a literature overview). Hence, typical f values are in the range of 4×10^{-4} to 2×10^{-3}, depending on the oxygen content of the wafer and the firing conditions (Ref. 1 reported a typical $f = 2 \times 10^{-6}$, but contained an error in physical units by three orders of magnitudes, and therefore that erroneous value corresponds to $f = 2 \times 10^{-3}$).

IV. CONCLUSION

In this study, we determined the amount of incomplete ionization of Al dopants in silicon by comparing ECV and micro Raman spectroscopy measurements of Al-doped Si surfaces. The resulting experimental data are clearly inconsistent with the pioneering theory of incomplete ionization from Pearson and Bardeen. Even the most recent parameterization could not be described satisfactorily. Therefore, new parameters for the most recent parameterization are proposed in Table I, considering well established values for boron-, phosphorus-, and arsenic-doped silicon. For device simulations, we recommend to use Eqs. (6) and (7) or Eqs. (3) to (5) with Table I to account for incomplete ionization, together with the accompanying reduction of band gap narrowing.

ACKNOWLEDGMENTS

The authors would like to thank Jonas Schön and Andreas Schenk for fruitful discussions. Michael Rauer wants to thank the Reiner Lemoine Stiftung for funding.

[1]P. Altermatt, S. Steingrube, Y. Yang, C. Sprodowski, T. Dezhdar, S. Koc, B. Veith, S. Herrman, R. Bock, K. Bothe, J. Schmidt, and R. Brendel, presented at the Proceeding of the 24th European Photovoltaic Solar Energy Conference, Hamburg, Germany, 2009, pp. 901–906.
[2]R. Bock, P. P. Altermatt, J. Schmidt, and R. Brendel, Semicond. Sci. Technol. **25**(10), 105007 (2010).
[3]J. Schmidt, N. Thiemann, R. Bock, and R. Brendel, J. Appl. Phys. **106**(9), 093707 (2009).
[4]M. Rüdiger, M. Rauer, C. Schmiga, and M. Hermle, J. Appl. Phys. **110**, 024508 (2011).
[5]T. F. Rosenbaum, R. F. Milligan, M. A. Paalanen, G. A. Thomas, R. N. Bhatt, and W. Lin, Phys. Rev. B **27**, 7509–7523 (1983).
[6]N. F. Mott, Rev. Mod. Phys. **40**, 677–683 (1968).
[7]P. P. Altermatt, A. Schenk, and G. Heiser, J. Appl. Phys. **100**(11), 113714 (2006).
[8]G. L. Pearson and J. Bardeen, Phys. Rev. **75**, 865–883 (1949).
[9]P. P. Altermatt, A. Schenk, B. Schmithusen, and G. Heiser, J. Appl. Phys. **100**(11), 113715 (2006).
[10]D. W. Fischer and J. J. Rome, Phys. Rev. B **27**(8), 4826–4832 (1983).
[11]R. L. Aggarwal and A. K. Ramdas, Phys. Rev. **140**, A1246–A1253 (1965).
[12]D. Karaiskaj, T. A. Meyer, M. L. W. Thewalt, and M. Cardona, Phys. Rev. B **68**, 121201 (2003).
[13]F. Huster and G. Schubert, presented at the Proceedings of the 20th European Photovoltaic Solar Energy Conference, Barcelona, Spain, 2005, pp. 1462–1465.
[14]E. Peiner, A. Schlachetzki, and D. Krüger, J. Electrochem. Soc. **142**(2), 576–580 (1995).
[15]P. Blood, Semicond. Sci. Technol. **1**(1), 7 (1986).
[16]F. D. Heinz, W. Warta, and M. C. Schubert, Energy Proc. **27**(0), 208–213 (2012).
[17]S. M. Sze, *Physics of Semiconductor Devices*, 2nd ed. (John Wiley & Sons, Inc., New York, 1981).
[18]P. T. Landsberg, Proc. Phys. Soc. Sec. A **65**(8), 604 (1952).
[19]P. P. Debye and E. M. Conwell, Phys. Rev. **93**, 693–706 (1954).
[20]L. Pincherle, Proc. Phys. Soc. Sec. A **64**(7), 663 (1951).
[21]G. Castellan and F. Seitz, presented at the Proceedings Conference, Butterworths, London, 1951.
[22]M. A. Green, J. Appl. Phys. **67**(6), 2944–2954 (1990).
[23]*Sentaurus Device User Guide, Version H-2013.03, Synopsys* (Zürich, Switzerland, 2013).
[24]P. T. Landsberg, Proc. Roy. Soc. London. Ser. A **213**(1113), 226–237 (1952).
[25]E. A. Guggenheim, Proc. Phys. Soc. Sec. A **66**(1), 121 (1953).
[26]G. A. Swartz, J. Phys. Chem. Solids **12**, 245–259 (1960).
[27]Y. Furukawa, J. Phys. Soc. Jpn. **16**, 577 (1961).
[28]R. Baron, G. A. Shifrin, O. J. Marsh, and J. W. Mayer, J. Appl. Phys. **40**(9), 3702–3719 (1969).
[29]M. Tajima, T. Masui, D. Itoh, and T. Nishino, J. Electrochem. Soc. **137**(11), 3544–3551 (1990).
[30]G. Galvagno, A. L. Ferla, F. L. Via, V. Raineri, A. Gasparotto, A. Carnera, and E. Rimini, Semicond. Sci. Technol. **12**(11), 1433 (1997).
[31]M. Rauer, M. Rüdiger, C. Schmiga, H. Strutzberg, M. Bähr, M. Glatthaar, and S. W. Glunz, J. Appl. Phys. **114**(20), 203702 (2013).
[32]T. Yoshikawa and M. Kazuki, J. Electrochem. Soc. **150**(8), G465–G468 (2003).
[33]M. Rauer, C. Schmiga, M. Hermle, and S. W. Glunz, presented at the Proceedings of the 24th European Photovoltaic Solar Energy Conference, Hamburg, Germany, 2009, pp. 1059–1062.
[34]J. Krause, R. Woehl, M. Rauer, C. Schmiga, J. Wilde, and D. Biro, Solar Energy Mater. Solar Cells **95**(8), 2151–2160 (2011).
[35]T. J. Woodley and C. T. Sah, Solid-State Electron. **20**(4), 385–388 (1977).

[36]U. Fano, Phys. Rev. **124**(6), 1866–1878 (1961).
[37]F. Cerdeira, T. A. Fjeldly, and M. Cardona, Phys. Rev. B **8**, 4734–4745 (1973).
[38]P. Lölgen, C. Leguijt, J. A. Eikelboom, R. A. Steeman, W. C. Sinke, L. A. Verhoef, P. F. A. Alkemade, and E. Algra, presented at the Proceedings of the 23rd IEEE Photovoltaic Specialists Conference, Louisville, Kentucky, USA, 1993, pp. 1490, 1236–1442.
[39]R. Bock, J. Schmidt, R. Brendel, H. Schuhmann, and M. Seibt, J. Appl. Phys. **104**(4), 043701 (2008).
[40]F. Huster, presented at the Proceedings of the 20th European Photovoltaic Solar Energy Conference, Barcelona, Spain, 2005, pp. 1466–1469.
[41]P. P. Altermatt, J. Comput. Electron. **10**(3), 314–330 (2011).
[42]A. Richter, S. W. Glunz, F. Werner, J. Schmidt, and A. Cuevas, Phys. Rev. B **86**(16), 165202 (2012).
[43]H. Mäckel and K. Varner, Prog. Photovolt. **21**(5), 850–866 (2013).
[44]R. Brendel, presented at the Proceedings of the 12th European Photovoltaic Solar Energy Conference, Amsterdam, The Netherlands, 1994, pp. 1339–1342.
[45]Y. Chen, H. Shen, and P. P. Altermatt, Solar Energy Mater. Solar Cells **120**(Part A), 356–362 (2014).
[46]P. Rosenits, T. Roth, and S. W. Glunz, Appl. Phys. Lett. **99**(23), 239904 (2011).
[47]A. Schenk, J. Appl. Phys. **84**(7), 3684–3695 (1998).
[48]B. Fischer, Ph.D. thesis, Universität Konstanz, Konstanz, Germany, 2003.